Journal of Molecular Modeling (2018) 24:2
https://doi.org/10.1007/s00894-017-3538-y

ORIGINAL PAPER

Double-layer carbon nanocapsules with radioiodine content and its interaction with calcium, phosphorus, and strontium

Alejandro Valderrama[1] · Radamés Reynoso[1] · Raúl W. Gómez[1] · Manuel Quintana[1] · Martín Romero[1]

Received: 5 February 2017 / Accepted: 15 November 2017
© Springer-Verlag GmbH Germany, part of Springer Nature 2017

Abstract

First principles calculations have been performed for $C_{60}@C_{180}$ carbon double-layer endofullerenes with up to: three diatomic radioiodine molecules ($^{131}I_2$), two potassium radio-iodide ($K^{131}I$), and three sodium radio-iodide ($Na^{131}I$) inside. The plane-wave pseudopotential (PP) method within the general gradient approximation (GGA) in the framework of the density functional theory (DFT) and time-dependent DFT (TD-DFT) was used to perform geometric optimizations (GOs) and molecular dynamics (MD) at 310 K and atmospheric pressure. We found that the double-layer carbon nanocapsules formed by two concentric fullerenes (C_{180} surrounding C_{60}) are very stable and may contain a radiodosis, without altering their configuration; that is, the $3(^{131}I_2)@C_{60}@C_{180}$, $2(K^{131}I)@C_{60}@C_{180}$, and $3(Na^{131}I)@C_{60}@C_{180}$ systems constitute stable nanocapsules. We analyzed the interaction of double-layer endofullerene with radioactive content with some calcium, phosphorus, and strontium atoms, $[n(X^{131}I)@C_{60}@C_{180} + mY]$, for X = I, K, Na; Y = Ca, P, Sr; $n = 1, 2, 3$; $m = 1, \ldots, 20$. Our calculations show that up to $m = 20$ calcium atoms can easily be physisorbed by the outer surface of the double-layer endofullerene, maintaining their integrity and shielding the radiodosis of any interaction that can proceed from the outside. It is thus concluded that these double-layer endofullerenes can be functionalized as vectors to deliver radiodosis with structural advantages over the single layer systems; as they are more robust, stable, and possess a larger surface to functionalize with some atoms serving as molecular recognizers.

Keywords Buckyball · C_{60} · Endofullerene · Nanocapsule · Radioiodine

Introduction

Cancer is one of the leading causes of mortality in the industrialized world [1]. The rapid multiplication of abnormal cells in a specific organ or tissue can fatally metastasize to the rest of the body [1–3]. Different treatments are required according to the initial organ or tissue affected. The treatments range from strengthening the immune system [4, 5] to the direct application of radioactive therapy, as for example, in the case of the thyroid cancer [6, 7]. The effectiveness of the treatment in this particular case resides in the natural affinity of this gland for iodine, which is easily absorbed from the bloodstream. Statistical studies determine the concentration of a radio dose to balance the abnormal growth of the thyroids cells. The extension of this successful statistical treatment to other tissues that could suffer the disease is desirable.

Currently, there is a wide variety of alternatives that consider nanoparticle formulations to target drug delivery against cancer which have improved therapeutic efficacy and clinical diagnosis [8, 9]. However, there are still many limitations related to the way in which recognition and cellular internalization actions can be performed [10].

Carbon nanotubes (CNTs) as multifunctional transporters can be used for radioactive iodine (RI) encapsulation and in this way to evade its natural affinity with thyroid gland and thus avoid its uptake. According to Sung You Hong and Gerard Tobias [11], this would allow the nanotubes to reach other specific areas of the body to combat tumors. Following this idea, it becomes necessary to tailor nanocapsules capable of containing a radiodosis and to travel in the bloodstream to perform the localized medication by molecular recognition of the different human tissues.

✉ Alejandro Valderrama
alecvald@ciencias.unam.mx

[1] Facultad de Ciencias, Universidad Nacional Autónoma de México, Avenida Universidad No. 3000, Ciudad Universitaria, C.P. 04510 Delegación Coyoacán, D.F., Mexico

Published online: 04 December 2017

Need for a double-layer nanocapsule

It has been proven in many works that nanotubes and fullerenes are able to encapsulate different atoms [12, 13], and that they also possess a good surface adsorption. However, the interaction with many atoms, inside or outside the carbon walls, may affect its configuration, its stability, and even its encapsulation capacity. Previous results [14, 15] show that fullerenes suffer cracks and stresses that may disrupt them when they are subjected to multiple interactions either from inside or outside.

Therefore, the use of nanocapsules to carry radioactive contents inside the body through the circulatory system needs a reliable architecture and geometry which can be based on the use of multilayer fullerenes: They need to be capable of encapsulating radioactive compounds (such as those used for the treatment of hyperthyroidism) and be stable when they interact with other atoms or molecules or determine whether its surface has been functionalized with molecular recognizers or tracers. Moreover, it is important to take into account the possible interaction of the nanocapsules with other substances present in the blood stream to ensure that they are robust enough to preserve their integrity and complete their mission.

The interaction between fullerene C_{60} and water molecules is hydrophobic [16, 17], even in solutions of sodium or potassium chloride, NaCl and KCl [18] respectively. Hence it is safe to consider that blood behaves in a similar way to water, since its composed of 90% of this element, so the interactions with the other components are small enough as to ignore them in a first approximation.

We have recently reported that carbon nanocapsules, although very strong and mechanically resistant, may present a redistribution of the electric charge that weakens some of the lattice bonds of the carbon structure when they contain some elements or compounds [19]. A further interaction over the outer surface with other atoms may simply break the already weakened bonds by the excess of charge. To overcome this problem, a nanocapsule can be shaped with two or more layers of fullerenes, what is known as nano-onions, which are considered as a promising future for biomedical applications. Different methods have been developed to synthesize nano-onions and their properties have been extensively studied [20]. It's well known that these carbon particles have a high cellular uptake, low cytotoxicity, and lower inflammatory potential than single or multi-walled carbon nanotubes (MWCNTs). According to their length, nanotubes may have an inadequate dispersal ability and insufficient excretion rates that prevents their accumulation in the organs of the human body [21].

In this study, we consider a double-layer nanocapsule. We simulate the C_{60} fullerene inside a larger C_{180} carbon fullerene, forming the molecular system of concentric fullerenes $C_{60}@C_{180}$ [22]. Thus, the largest fullerene will have the function of shielding the interaction forces from other atoms or molecules from the outside and the C_{60} fullerene may contain a radioactive dose which will then be protected inside the double-layer system.

Ideally both layers formed by the fullerenes C_{60} and C_{180} of the double-layer nanocapsule must interact weakly with each other, so that a practically neutral space is created between them. The C_{60} fullerene inside the C_{180} will store some compound in its central neutral zone, which will be protected from possible outside random interactions. Finally, the double-layer nanocapsule must be able to maintain its integrity in the blood stream until it arrives at the end of its journey to apply the radioactive dose. In consequence, once a double-layer endofullerene nanocapsule is attained, it will be of interest to test the capability of its outer layer to physisorb atoms of different types. For example, calcium, phosphorus, and strontium could be used as a system test for bone tissue recognition given its affinity to its mineral components.

Computational methods

The methodology used in this work is based on the application of the functional density theory (DFT) and time-dependent DFT (TD-DFT) [23–25]. We have performed first-principles calculations and determined, for the molecular systems studied: C_{60}, C_{180}, $n(X^{131}I)$ were X = I, K, Na and $n = 1, 2, 3$; its composition as endofullerenes with radioactive content, its interactions with some calcium, phosphorus, and strontium atoms and their energies in the fundamental state. Geometric optimizations (GOs) obtained and all the molecular dynamics (MD) [26] were performed with the code for the MPI parallel processing Quantum Espresso (QE) [27] version 5.0.2 running pw.x up to 256 microprocessors (MPs) at 2.5 Ghz in the self-consistent mode (PWscf). We applied the Born-Oppenheimer method and generalized gradient approximations (GGA) [28] for the correlation and exchange energies of Perdew-Burke-Ernzerhof (PBE) with a norm conservation pseudopotential (PP) [29] of Martins-Troullier's type [30].

The energies of the structures were calculated in unrestricted mode by taking, in the initial configuration, the valence electron states: 4 for carbon, $_6$C: [He] $2s^2 2p^2$; 1 for sodium, $_{11}$Na: [Ne] $3s^1$; 5 for phosphorus, $_{15}$P: [Ne] $3s^2\ 3p^3$; 1 for potassium, $_{19}$K: [Ar] $4s^1$; 10 for calcium, $_{20}$Ca: [Ar] $3s^2 3p^6 4s^2$; 10 for strontium (because the $4s^2$ and $4p^6$ are taken into account by the PP), $_{38}$Sr: [Kr] $5s^2$; and 7 for iodine, $_{53}$I: [Kr] $4d^{10} 5s^2 5p^5$. The cut-off energy for PPs approximation with plane wave functions was 544.22 eV. An automatically calculated grid of k points in the Brillouin space was used for the integration of the electronic structure. The Methfessel-Paxton approximation [31] for the occupation numbers with a value of 0.07 eV was used for faster convergence along the

three perpendicular directions. The energy convergence threshold was taken at 0.1 meV. Total energy and electronic structure calculations were performed with estimated SCF accuracy $<9.0 \times 10^{-5}$ eV. These parameters have been shown to be very efficient for the study of surface adsorption systems [32, 33]. In the case of the MD, the systems followed an evolutionary process using a scaling up of velocities until they attain 310 K, maintaining a one atmosphere pressure and considering the minimum interval (time step) ≅ 1 f-second (*fs*). The pressure in the Quantum Espresso code is controlled by adding degrees of freedom for cell size and volume with an application of the Lagrangian Parrinello-Rahman [34].

For the molecular systems studied, the formation energy was determined as the difference of the values of the energies of the complete system minus the sum of the energies of its components; that is:

$$E_f = E_T\left[n\left(X^{131}I\right)@C_{60}@C_{180}\right)\Big] - \left[180E_T(C) + 60E_T(C) + nE_T\left(X^{131}I\right)\right], \textit{with } X = I, K, Na \textit{ and } n = 1, 2, 3.$$

Where, $E_T[n(X^{131}I)@C_{60}@C_{180}]$ is the final configuration energy of the composite system in the fundamental state and $[180E_T(C) + 60E_T(C) + nE_T(X^{131}I)]$ is the energy of 180 + 60 = 240 carbon atoms of a gas without interaction between particles, plus the energy of n isolated molecules of $(X^{131}I)$. Thus, with $n = 0$ we have the empty double-layer fullerene and we take the average bond energy as: $<E_A> = E_f / 240$.

For $n = 1$, 2 or 3 there would be a double-layer endofullerene containing 1, 2 or 3 radioactive iodine molecules, with $3(^{131}I_2)$, $2(K^{131}I)$, and $3(Na^{131}I)$ being the maximum number of molecules that a C_{60} fullerene can contain without breaking, as the images show in the following series of computational simulations with the final configurations of the GOs obtained; we have reported some of these systems earlier [15] (Fig. 1).

n($X^{131}I$)@C60 DFT geometric optimizations

With the results obtained from the encapsulation capacity of radioactive iodine molecules inside the C_{60} fullerene, we find for the composite double-layer systems with $n = 1$, 2 or 3 molecules of $(X^{131}I)$ contained in the fullerene that the encapsulation energy per molecule is: $<E_A> \approx 2 * E_f / (240 + 2n)$, since each $(X^{131}I)$ has two atoms, and assuming that its cohesive energy is

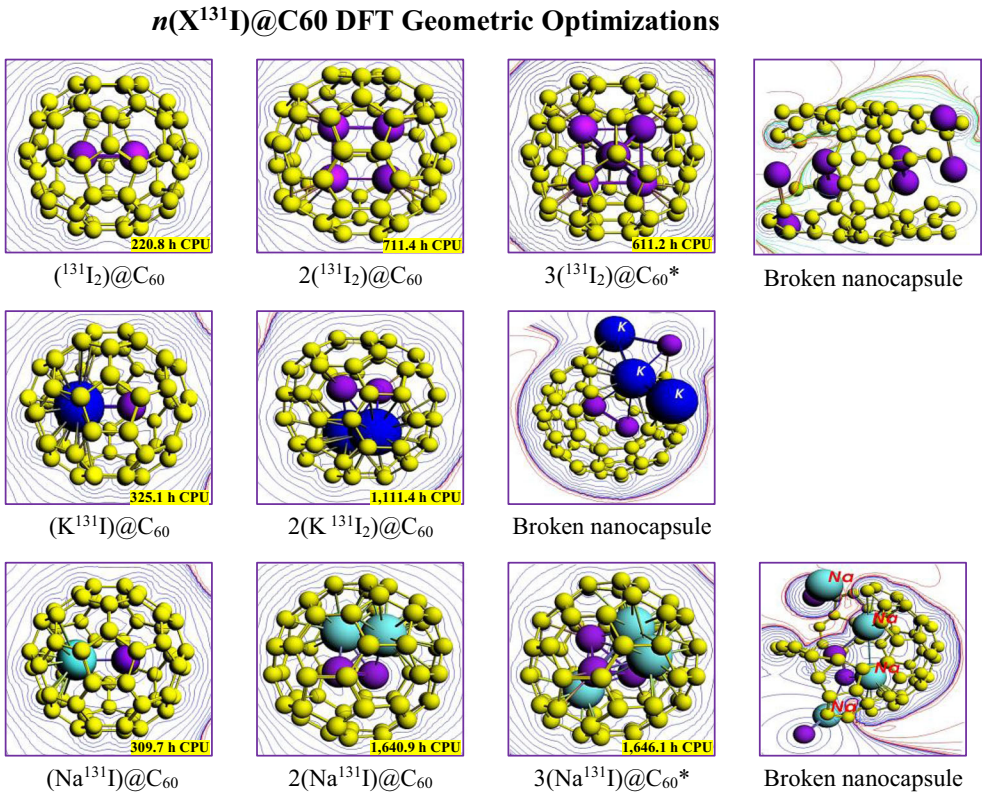

Fig. 1 In the series of images (calculated with parallel version of MPI on 256 MPs) is observed how, as the number of molecules contained inside the fullerenes increases, they begin to expand until breaking. The encapsulation limit found for $^{131}I_2$, $K^{131}I$, and $Na^{131}I$ molecules are: $3(^{131}I_2)$, $2(K^{131}I)$, and $3(Na^{131}I)$. The obtained values for the fundamental state energies are listed in Table 2

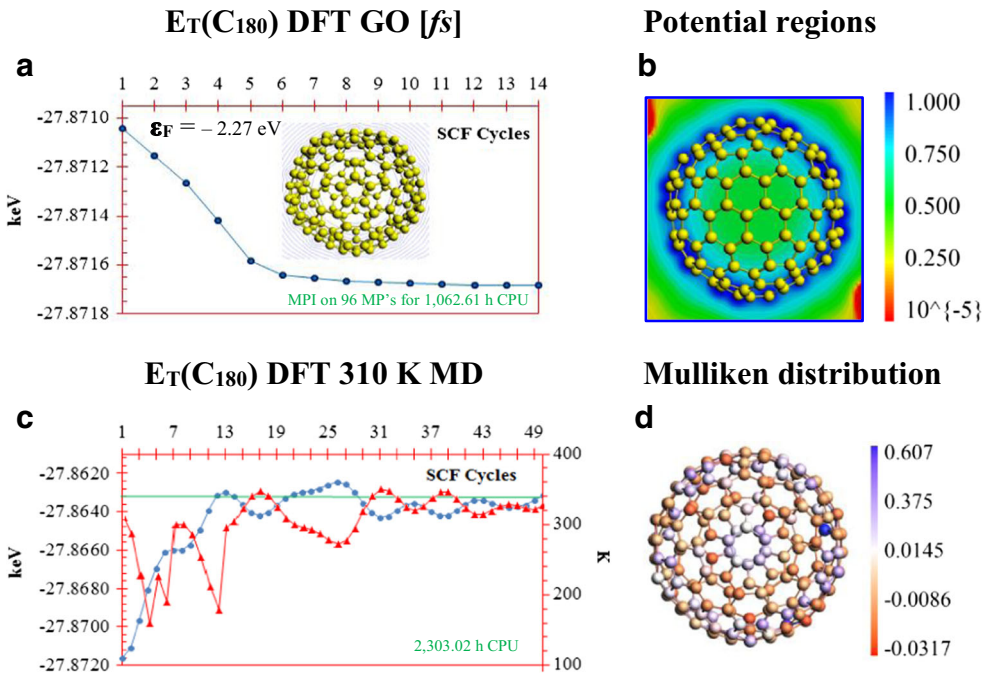

Fig. 2 a) Convergence of the total energy, E_T [keV], of the C_{180} system to the fundamental state during the relaxation process and the Fermi energy, ε_F [eV], obtained. The fullerene C_{180} representation shows the equipotential lines SCF of the molecular structure. b) In the fullerene field representation, the dark blue areas show a positive potential while the green illuminated areas show a practically neutral potential. The scale is normalized. c) The graph shows the MD for the C_{180} fullerene, E_T [keV] in blue and temperature [K] in red. The first 50 cycles of SCF or clock cycles with units of the order of femto-seconds (*fs*) are presented (the processing time for the calculus required more than 2300 h CPU), starting from the point of relaxation until reaching 310 K, at a constant pressure of 1 atm. Fullerene C_{180} is maintained in a state of stable vibration during the simulation of the heating, without losing its integrity or presenting cracks. d) In the fullerene representation, the charges are colored according to their Mulliken's distribution in a balanced way

approximately the same as the other atoms in the system. The calculated results are presented below.

As a parameter of additional molecular characterization included in the methodology, in all the systems studied, we performed calculations of the relativistic scalar type of polarized and non-polarized spin. In both cases, we obtained identical results by which we establish that these systems are not magnetic. The molecular graphic representations were made with the Scientific Computing & Modeling ADF release 2009.01 software.

Results and discussion

Although C_{180} and double layer $C_{60}@C_{180}$ fullerenes have been previously studied [22], we have performed the corresponding calculations as a starting point, since our objective is to study the latter's ability to transport radiodosis of $n(X^{131}I)$ molecules, with X = I, K, Na and $n = 1, 2, 3$, without disrupting or cracking when coming into contact with other atoms. We are also interested in their capability to physisorb, on their outer surface, calcium, phosphorus or strontium atoms that may well be used as molecular recognizers of specific tissues such as bone. We present below the results obtained for the simple and compound systems.

The C_{180} fullerene

A fullerene that can properly enclose the C_{60} buckyball, which has an approximate radius of 6.78 Å, is the C_{180}, with a radius between 12.65 to 12.70 Å, resulting suitable to form a double-layer nanocapsule. The geometric coordinates of the atoms in this structure were acquired with the free version of Nanotube Modeler© JCrystalSoft (Fullerenes Library) software. The C_{180} fullerene is a convex polyhedron of 77 faces consisting of a spherical array of atoms occupying the vertices of 65 hexagons and 12 pentagons, where the latter do not share any edges. In the C_{180} fullerene, the carbon bonds range from 1.38 to 1.43 Å, so they are very close to those of C_{60}.

In an analogous way to the case for the C_{60} fullerene, the corresponding simulations were performed for C_{180}. The relaxation of the C_{180} structure was also calculated using supercomputing type process with the parallel processing QE code for the DFT calculations. For the energy functional, we used the same pseudopotential PBE exchange-correlation scalar relativistic which includes an approximation with ultrasoft functions using the Martins-Troullier method. The obtained results for the energy values: total, of formation, average binding per particle, and its Fermi energy corresponding to the highest level occupied are listed in Table 2. The convergence was reached quickly, after only 14 cycles of SCF calculation

or 14 *fs* in molecular time terms (although the processing time for the calculus required more than 1000 h CPU), as can be seen in the graph of Fig. 2a). The fullerene's total energy variation is ten thousandths of keV, that is, less than 0.1 eV. The configuration obtained for the C_{180} after the relaxation differs very little from the initial atom positions obtained from the fullerenes coordinate library. Thus, again the efficacy of the method and pseudopotential used for the relaxation calculations at the fundamental state is verified. In a similar way, in the MD of C_{180} at 310 K and atmospheric pressure we obtained a stable state; the results are shown in Table 2.

In MD, the total energy is defined by $E_T = E_{potential} + E_{kinetic}$; it was calculated at 310 K obtaining $E_{kinetic} = 7.5285$ eV. The ground state energy in the molecular dynamics differs by 0.012% from that obtained in the corresponding GO, which is less than one thousandth. So, the system at this temperature does not undergo significant changes; the graph in Fig. 2c shows the evolution of molecular dynamics and in d) a stability condition based on the Mulliken charge distribution.

$C_{60}@C_{180}$ double-layer nanocapsule

Next, we present the results obtained for the new system formed by the C_{60} surrounded by the C_{180} fullerene. The pseudopotential used for relaxation is the same as that used in previous cases. It is interesting to note that in the composite structure practically the same average binding energy per particle is preserved, so the system is well constituted and is a robust system, see Table 2. This is verified by observing the small differences between the energy of the coupling and the energy of the fragments: $E_f = E_T[C_{60}@C_{180}] - (180E_T[C] + 60E_T[C])$. Thus, this set of 240 carbon atoms constitutes a very stable multilayer nanocapsule.

The graph in Fig. 3 shows the convergence of the system to the ground state. As can be seen, the distribution of the positive and neutral regions of both fullerenes is such that an excellent fit is obtained, leaving the buckyball C_{60} well located in the neutral inner part of the C_{180} fullerene.

Figure 3b) shows that the surfaces of the two fullerenes have a slightly positive electrical potential, so they repel; thus, the C_{60} buckyball is confined to the central part of the C_{180} fullerene. This situation does not change much with the increase in temperature, as shown in the results obtained from the molecular dynamics of $C_{60}@C_{180}$ to 310 K in Table 1. The energy of the ground state in MD differs by 0.02% from that obtained in the corresponding GO, which is less than one thousandth. Therefore, the system at this temperature does not show significant changes and remains stable.

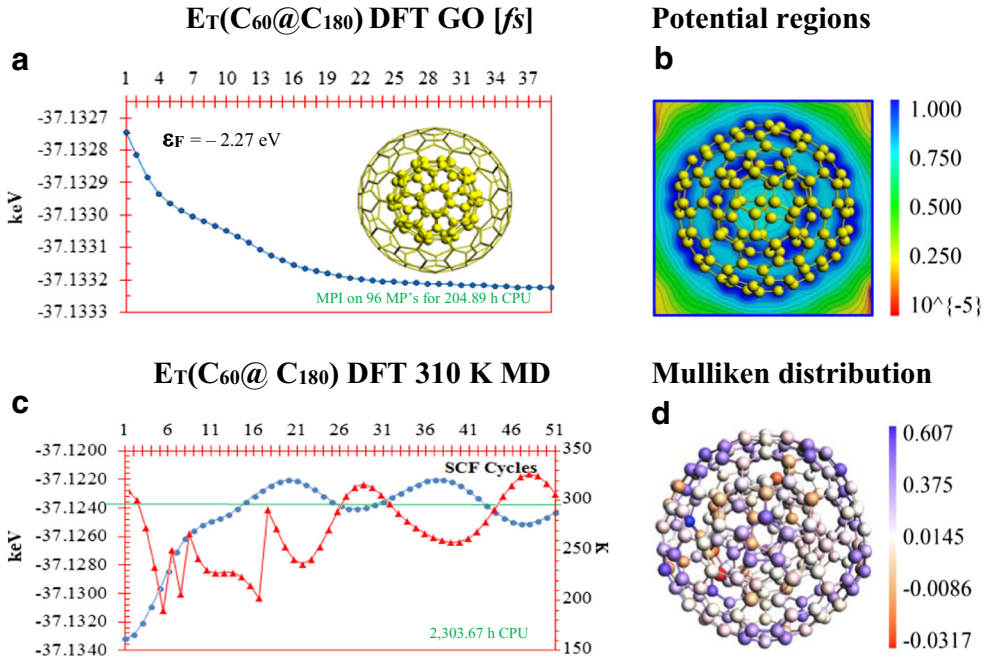

Fig. 3 a) The graph shows the convergence of the E_T [keV] to the fundamental state and the ε_F [eV] obtained. In the representation of the $C_{60}@C_{180}$ the atoms of the outer sphere C_{180} were removed to facilitate the visualization of the assembly. b) This figure also shows dark blue regions of positive potential and regions in light blue of practically neutral potential. c) The graph shows the MD for the $C_{60}@C_{180}$ fullerene, E_T [keV] in blue and temperature [K] in red. The first 51 cycles of SCF or clock cycles with units of the order of femtoseconds (*fs*) are presented (the processing time for the calculus required more than 2300 h CPU), starting from the point of relaxation until reaching 310 K, at a pressure of 1 atm. As in the previous case, the double-layer fullerene $C_{60}@C_{180}$ is maintained in a state of stable vibration during the simulation of the heating, without losing its integrity or presenting cracks. d) In the fullerene representation, the charges are colored according to their Mulliken's distribution in a balanced way

Table 1 Average and maximum distances between near carbon atoms

Bond lengths [Å]	C_{60}		C_{180}	
	<d(C−C)>	$<d_M(C-C)>$	<d(C−C)>	$<d_M(C-C)>$
C_{60}	1.439	1.459		
$3(^{131}I_2)@C_{60}$	1.545	1.687		
$2(K^{131}I)@C_{60}$	1.481	1.542		
$3(Na^{131}I)@C_{60}$	1.512	1.600		
C_{180}			1.426	1.465
$C_{60}@C_{180}$	1.477	1.514	1.451	1.485
$3(^{131}I_2)@C_{60}@C_{180}$	1.503	1.630	1.457	1.518
$2(K^{131}I)@C_{60}@C_{180}$	1.446	1.516	1.451	1.504
$3(Na^{131}I)@C_{60}@C_{180}$	1.474	1.595	1.438	1.512

Double-layer nanocapsule with radioactive content

Once the configuration of the multilayer nanocapsule $C_{60}@C_{180}$ was found, we simulated the same nanocapsule, but with three diatomic molecules of iodine-131, ($^{131}I_2$); two molecules of ($K^{131}I$), and three molecules of ($Na^{131}I$). The geometric optimization was carried out with the same method as for the previous cases. We used the same pseudopotential for carbon and iodine respectively since they have proven that they can be transferred effectively. The results for the GOs of the $n(X^{131}I_2)@C_{60}@C_{180}$ systems obtained are shown in Table 2. Next, the graphs show the convergence of the systems to the fundamental state. As shown in Fig. 4b), d), and f) the $3(^{131}I_2)@C_{60}@C_{180}$, $2(K^{131}I)@C_{60}@C_{180}$, $3(Na^{131}I)@C_{60}@C_{180}$ systems constitute stable multilayer nanocapsules with radioactive content, in which the outer fullerene C_{180} provides shielding to the "vulnerable" endofullerene $n(X^{131}I)@C_{60}$.

Because both fullerenes interact very little with each other, there are no significant changes in the composite configuration (see results in Table 2). The stability of the system is verified again with the small difference between the energy of coupling and the energy of the fragments, that can be easily calculate with the expression: $E_f = E_T[n(X^{131}I)@C_{60}@C_{180}] - E_T[C_{180}] - E_T[n(X^{131}I)@C_{60}]$.

Bond length averages

With the previous simulations the average lengths of the carbon bonds of the studied systems are easily obtained, being

Table 2 Energy values: total, of formation, average binding per particle, and the Fermi energy corresponding to the highest level occupied (in molecular dynamics MD at 310 K and atmospheric pressure)

System	E_T [keV]		E_f [keV]		$<E_A>$ [eV]		ε_F [eV]
	GO	MD	GO	MD	GO	MD	GO
C_{60}	≅ − 9.279	≅ − 9.277	≅ − 0.427	≅ − 0.424	= − 7.126	= − 6.973	= − 4.57
$1(^{131}I_2)@C_{60}$	≅ − 9.895	≅ − 9.893	≅ − 0.421	≅ − 0.419	= − 6.790	= − 6.752	= − 4.06
$2(^{131}I_2)@C_{60}$	≅ − 10.489	≅ − 10.492	≅ − 0.392	≅ − 0.395	= − 6.127	= − 6.170	= − 4.05
$3(^{131}I_2)@C_{60}$ *	≅ − 11.083	≅ − 11.080	≅ − 0.362	≅ − 0.360	= − 5.493	= − 6.170	= − 3.81
$1(K^{131}I)@C_{60}$	≅ − 9.596	≅ − 9.591	≅ − 0.420	≅ − 0.415	= − 6.781	= − 6.700	= − 4.13
$2(K^{131}I)@C_{60}$ *	≅ − 9.901	≅ − 9.896	≅ − 0.400	≅ − 0.396	= − 6.261	= − 6.183	= − 4.07
$1(Na^{131}I)@C_{60}$	≅ − 9.600	≅ − 9.598	≅ − 0.423	≅ − 0.426	= − 6.823	= − 6.784	= − 4.28
$2(Na^{131}I)@C_{60}$	≅ − 9.911	≅ − 9.908	≅ − 0.407	≅ − 0.405	= − 6.362	= − 6.324	= − 4.05
$3(Na^{131}I)@C_{60}$ *	≅ − 10.210	≅ − 10.208	≅ − 0.381	≅ − 0.378	= − 5.767	= − 5.730	= − 3.96
C_{180}	≅ − 27.872	≅ − 27.865	≅ − 1.318	≅ − 1.312	= − 7.325	= − 7.287	= − 3.27
$C_{60}@C_{180}$	≅ − 37.133	≅ − 37.124	≅ − 1.729	≅ − 1.720	= − 7.204	= − 7.167	= − 2.27
$3(^{131}I_2)@C_{60}@C_{180}$	≅ − 38.957	–	≅ − 1.678	–	= − 6.821	–	= − 1.72
$2(K^{131}I)@C_{60}@C_{180}$	≅ − 37.784	–	≅ − 1.330	–	= − 5.451	–	= − 2.00
$3(Na^{131}I)@C_{60}@C_{180}$	≅ − 38.089	–	≅ − 1.326	–	= − 5.390	–	= − 1.92

*Encapsulation limit of this substance inside fullerene C_{60}

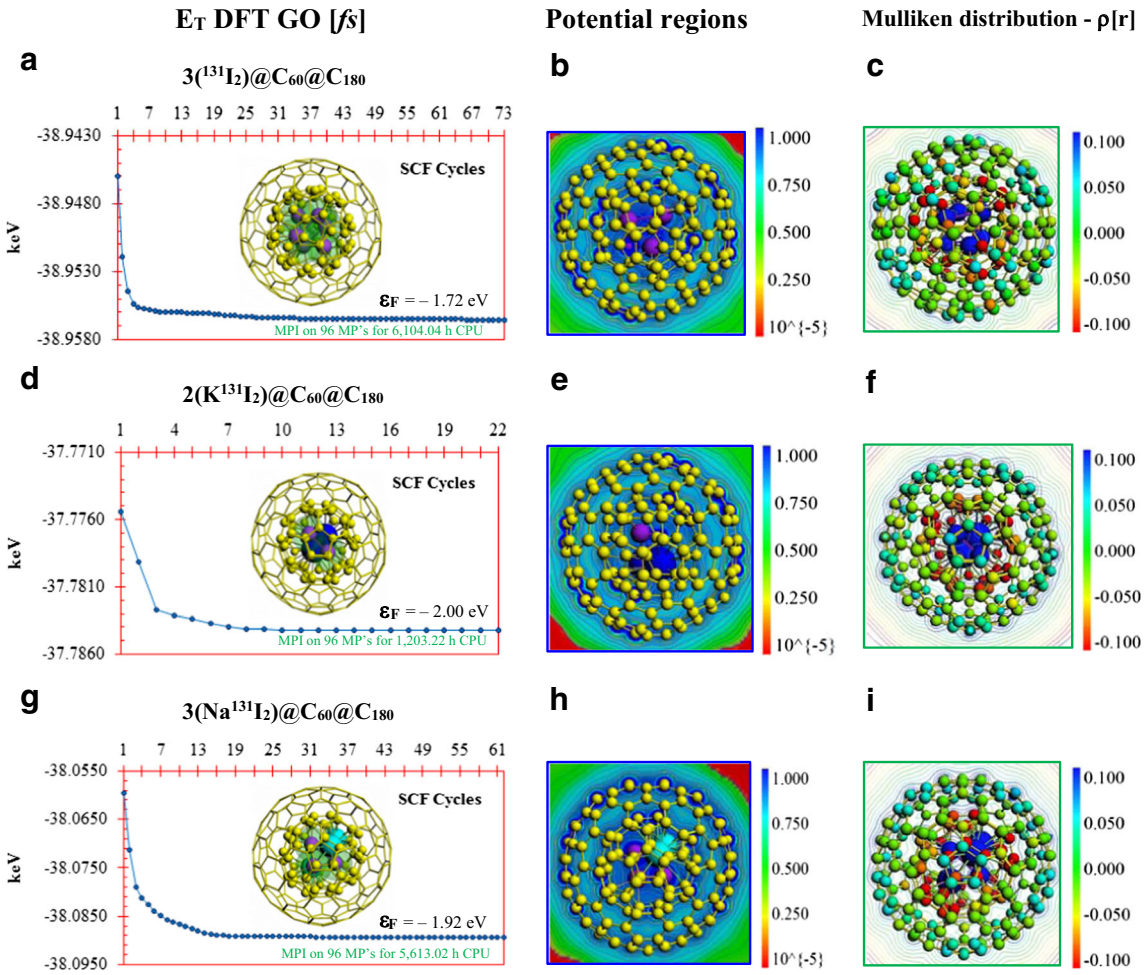

Fig. 4 a), d), g) Graphs show a rapid convergence of the E_T [keV] to the fundamental state and the final ε_F [eV] obtained. In the representations of $n(X^{131}I)@C_{60}@C_{180}$ the atoms of the outer sphere were removed so that the interior can be better appreciated. The region with radioactive iodine was illuminated to improve its visualization. b), e), and h) The regions of positive potential are shown in dark blue and those of neutral potential in light blue; and the scale is normalized. c), f), and i) show de Mulliken charge distribution and the electronic density field

smaller than 1.7 Å there are still the double or simple covalent bonds (The average carbon bond length is 1.44 Å. [35]) so there are no ruptures in any of the layers of the nanocapsule neither by its conformation nor by its content.

The following table shows the average and maximum distances between the carbon atoms of the simulated fullerenes. Data shows that the C_{60} fullerene undergoes expansion by containing some molecules of ($^{131}I_2$) or ($K^{131}I$) or ($Na^{131}I$) inside, this is because a fraction of the electric charge of the content is transferred to the carbons. The second layer, fullerene C_{180} slightly counteracts the expansive action (Fig. 5).

Interaction of the double-layer nanocapsule with calcium

Given the fundamental state of the double-layer nanocapsule with radioactive iodine content, we tested its interaction with the composite systems with up to 20 calcium atoms (Ca) as if they were free in the medium at the nanocapsule proximities [36]. For these, the GOs were carried out with the same methodology and PPs previously used [15]. The relaxation results of the $[n(X^{131}I)@C_{60}@C_{180} + 20Ca]$, X = I, K, Na; and n up to 3, systems are shown in Table 2.

The following figures show the simulated systems in the fundamental state. As can be seen, the interaction of the double-layer nanocapsule $n(X^{131}I)@C_{60}@C_{180}$ with 20 calcium atoms, as if they are free in the medium, results in the adsorption of these calcium atoms on the surface of the outer sphere of fullerenes C_{180}; results are listed in Table 2.

The single point energy of the calcium atom becomes – 1.015 keV, so that multiplying this by 20 atoms yields – 20.294 keV, which is its associated total energy. When comparing the total energy of the systems, $E_T[n(X^{131}I)@C_{60}@C_{180} + 20Ca]$ with that of the fragments, $E_T[n(X^{131}I)@C_{60}@C_{180}] + E_T[20Ca]$, the adsorption energy of the calcium atoms on the surface of the fullerene C_{180} is obtained with the simple difference. See results in Table 3.

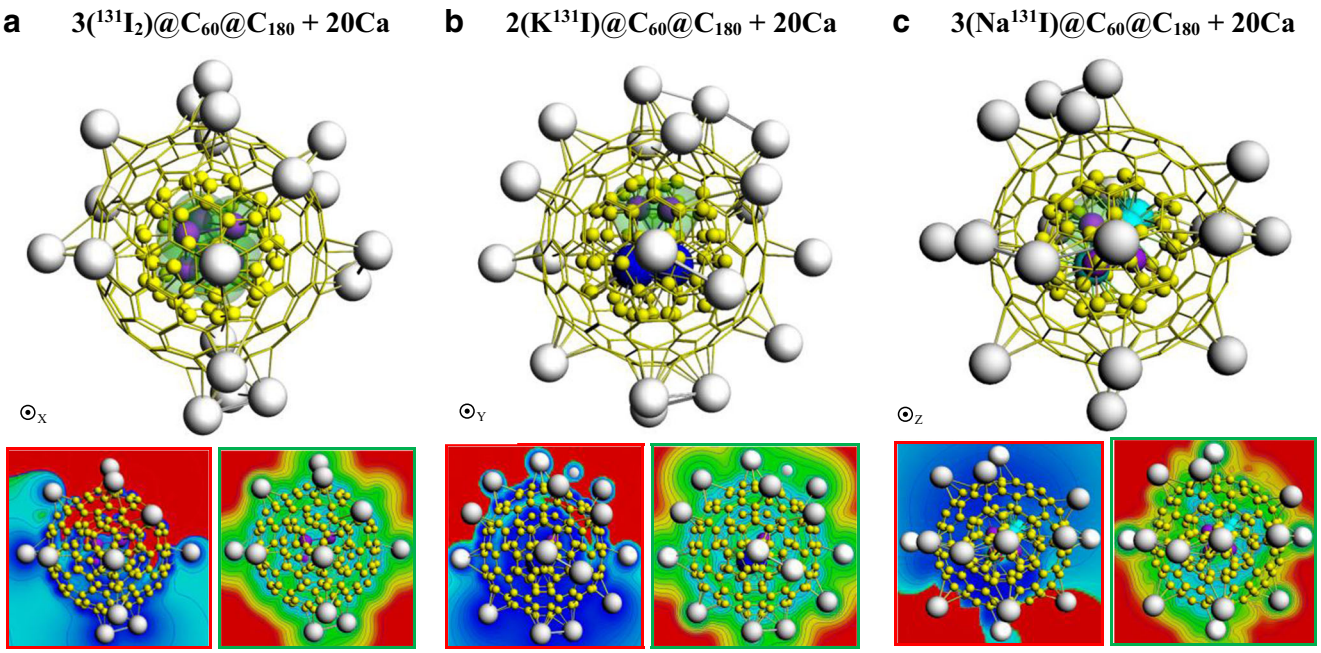

Fig. 5 a), b), c) At the top, the representations of the convergence to the fundamental state of the $n(X^{131}I)@C_{60}@C_{180}$ systems interacting with 20 Ca atoms, from the outer sphere C_{180} the carbon atoms have been removed to make the inner sphere more appreciable. The region with radioactive iodine $3(^{131}I_2)$, $2(K^{131}I)$, and $3(Na^{131}I)$ was illuminated to improve its visualization. At the left bottom, positive regions are also shown in dark blue, neutral potential in light blue, and a region of negative potential in red. Electronic density field maps are shown in the bottom right corner; the scale is normalized [$10^{-}5$,1]

Thus, the double-layer nanocapsule maintains its stability and the configuration of its atoms remains practically constant. The inner sphere efficiently stores radioactive iodine and the outer sphere generates the necessary shielding to maintain the integrity of the system while adsorbing calcium atoms on its surface. The external potential of the system is modified, which is evidenced with the appearance of a negative region in one of the hemispheres of the molecular system. This gives a polarization effect that could make the system more reactive.

Energy averages

In the simulations, the energy value changes are consistent with our double layer endofullerene model as summarized in Table 2. The formation and binding energies per particle are practically maintained in all systems. As shown in the table, the values of ε_F for all systems are of the order of electron volts so they have low thermal conductivity and low electrical conductivity.

For the composite systems, no molecular dynamics were performed since it has been previously tested that the components did not present significant changes in the temperature range of interest.

As can be seen in Table 3, the calcium surface physisorption results in a polar binding energy that is less than the average binding per particle but enough to maintain some calcium atoms added to the fullerene exterior surface. Thus again, it is verified that the nanocapsules have a good ability to adsorb atoms in their external surface maintaining its structural integrity.

Mulliken electronic charge distributions

It is interesting to do comparative analysis of the Mulliken electronegativity distribution [37] for calcium adsorption under similar simulation conditions for phosphorus and strontium. As can be seen in Tables 4, 5, and 6 the shielding effect works correctly. The electric response of the inner fullerene is for iodine molecules in most cases and the fullerene C_{180}'s

Table 3 Interaction of the $n(X^{131}I)@C_{60}@C_{180}$ systems with 20 calcium atoms; total adsorption $E_{A(20Ca)}$ and per atom of calcium $E_{A(Ca)}$ energies

System	E_T + 20Ca [keV]	E_T [keV]	20 Ca [keV]	$E_{A(20Ca)}$ [keV]	$E_{A(Ca)}$ [eV]	ε_F [eV]
$3(^{131}I_2)@C_{60}@C_{180}$	≅ − 59.278	≅ − 38.957	= − 20.294	= − 0.027	= − 1.35	= 0.54
$2(K^{131}I)@C_{60}@C_{180}$	≅ − 58.107	≅ − 37.784	= − 20.294	= − 0.029	= − 1.45	= 0.38
$3(Na^{131}I)@C_{60}@C_{180}$	≅ − 58.385	≅ − 38.089	= − 20.294	= − 0.002	= − 0.10	= 0.44

Table 4 Single point electronegativity charge distribution, in Mulliken's relative scale, of $3(^{131}I_2)@C_{60}@C_{180}$ interacting with 20 atoms of calcium, phosphorus, and strontium

System	$3(^{131}I_2)@C_{60}@C_{180}$ + 20Ca		$3(^{131}I_2)@C_{60}@C_{180}$ + 20P		$3(^{131}I_2)@C_{60}@C_{180}$ + 20Sr	
	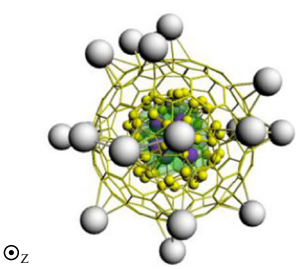		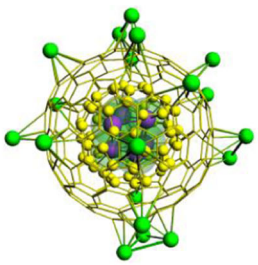		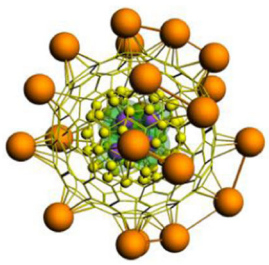	
Fraction	Total	Per atom	Total	Per atom	Total	Per atom
$3(^{131}I_2)$	5.3075	0.8846	4.4796	0.7466	6.4756	1.0793
C_{60}	-5.2698	– 0.0878	– 3.4634	– 0.0577	– 6.5332	– 0.1089
C_{180}	– 19.0744	– 0.1060	– 9.3760	– 0.0521	– 22.7152	– 0.1262
20 Y	19.0360	0.9518	8.3602	0.4180	22.7732	1.1387
ρ[r]	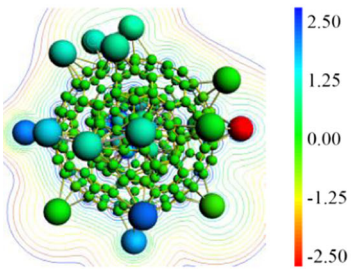		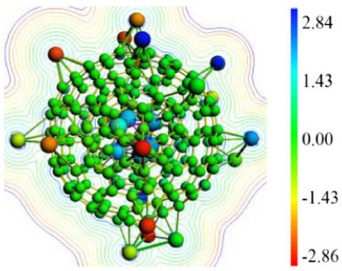		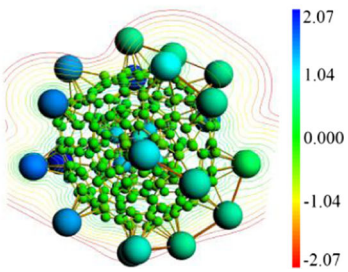	

response to atoms that interact on the outside. This shows that endo fullerenes respond well to interactions since they have the ability to accept or transfer negative electrical charge when interacting with other elements.

Table 5 Single point electronegativity charge distribution, in Mulliken's relative scale, of $2(K^{131}I)@C_{60}@C_{180}$ interacting with 20 atoms of calcium, phosphorus, and strontium

System	$2(K^{131}I)@C_{60}@C_{180}$ + 20Ca		$2(K^{131}I)@C_{60}@C_{180}$ + 20P		$2(K^{131}I)@C_{60}@C_{180}$ + 20Sr	
Fraction	Total	Per atom	Total	Per atom	Total	Per atom
$2(K^{131}I)$	9.3718	2.3430	7.4799	1.8700	6.8044	1.7011
C_{60}	– 4.4841	– 0.0747	– 8.1175	– 0.1353	– 15.5686	– 0.2595
C_{180}	– 18.0103	– 0.1001	– 6.9333	– 0.0385	16.3211	0.0907
20 Y	13.1223	0.6561	7.5703	0.3785	– 7.5563	– 0.3778
ρ[r]	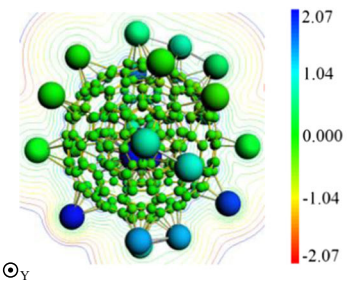		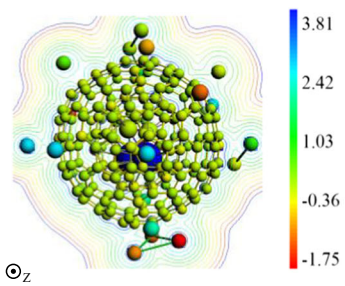		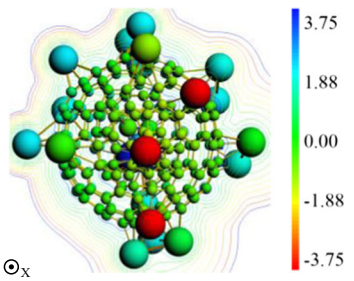	

Table 6 Single point electronegativity charge distribution, in Mulliken's relative scale, of $3(Na^{131}I)@C_{60}@C_{180}$ interacting with 20 atoms of calcium, phosphorus, and strontium

System	$3(Na^{131}I)@C_{60}@C_{180}$ + 20Ca		$3(Na^{131}I)@C_{60}@C_{180}$ + 20P		$3(Na^{131}I)@C_{60}@C_{180}$ + 20Sr	
Fraction	**Total**	**Per atom**	**Total**	**Per atom**	**Total**	**Per atom**
$3(Na^{131}I)$	9.0861	1.5144	8.9243	1.4874	9.1926	1.5321
C_{60}	– 8.3148	– 0.1386	-15.7023	-0.2617	– 9.3070	– 0.1551
C_{180}	– 16.0849	– 0.0894	-12.8275	-0.0713	– 23.1091	– 0.1284
20 Y	17.7476	0.8874	19.6047	0.9802	23.2238	1.1612
ρ[r]	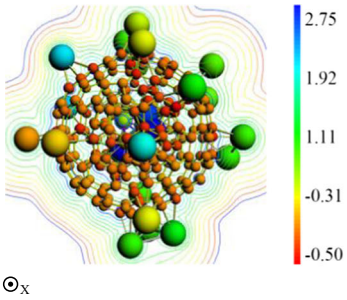		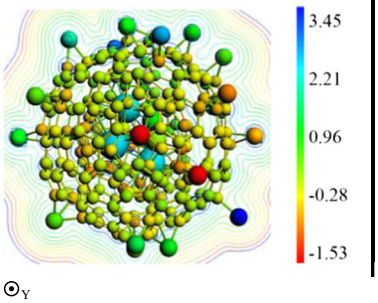		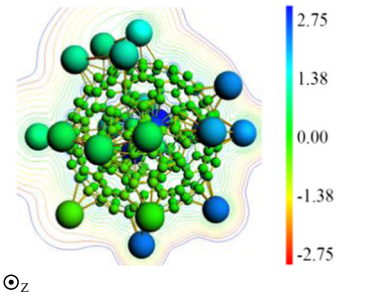	

Electronegativity analyses show interesting behavior of the physisorbed atoms as they rearrange their electrical charges to form systems polarly bonded by van der Waals forces. In almost all cases the charge layered distribution can be appreciated. However, some variants are also observed as in the case of the system $[2(K^{131}I)@C_{60}@C_{180} + 20Ca]$ in which negative charge is transferred from the potassium, at the center, to fullerenes C_{60} and C_{180} that provides greater shielding toward the outside.

Conclusions

The stability properties of single and double-layer endo-fullerenes, with DFT and TD-DFT, when they contain radioactive iodine compounds and interact with calcium, phosphorus, and strontium atoms were studied. Our results confirm that so-composed systems are weakly affected by changes in temperature in the region of less than 310 K which is the approximate human body temperature. This confirms the viability to use these systems as a platform for the delivery of radio doses.

We conclude that encapsulated radioactive elements in double-layer fullerenes, such as the $C_{60}@C_{180}$, are very good choices given their resistance and stability to carry compounds that can be used as cancer medication. Also, they will better withstand the interaction with different atoms and compounds in their journey through the bloodstream.

The physisorption of calcium atoms by the endofullerene with radioactive content suggests the possibility of including them in the bone metabolism. The calcium recognizers could have a good affinity with the molecules of hydroxyapatite that constitute the mineral component of the bones.

In addition, it is expected that other isotopes of phosphorus (^{32}P) or strontium (^{89}Sr) can be used in a similar way on the outer surface of the nanocapsule. These elements will modify the nanocapsule chemical affinity to serve as markers that can be tracked in their way to predetermined tissues, such as bone tissue itself, via the circulatory system, without affecting the inner nanocapsule which carries the radiodosis.

In summary, our results illustrate that a double-layer nanocapsule is suitable to transport radiodosis to some specific tissues because it is more interaction resistant with other atoms than its components separately, and it can adsorb atoms that have affinity with predetermined tissues.

Acknowledgements Thanks to Consejo Nacional de Ciencia y Tecnología for the financial support given to this work in the national postdoctoral program, to FAM Laboratory of Science Faculty and to Miztli Supercomputer Center of the Dirección General de Tecnologías de la Información y Comunicación of the Universidad Nacional Autónoma de México; and to the Laboratorio Nacional de Supercómputo del Sureste de México of the Benemérita Universidad Autónoma de Puebla for their technical support on many of the computations performed.

References

1. Howlader N, Noone AM, Krapcho M, Miller D, Bishop K, Altekruse SF, Kosary CL, Yu M, Ruhl J, Tatalovich Z, Mariotto A, Lewis DR, Chen HS, Feuer EJ, Cronin KA (eds) SEER Cancer Statistics Review, 1975-2013, National Cancer Institute. Bethesda, MD, http://seer.cancer.gov/csr/1975_2013/, based on November

2015 SEER data submission, posted to the SEER web site, April 2016. https://seer.cancer.gov/csr/1975_2013/. http://www.nature.com/cr/journal/v27/n1/full/cr2016153a.html
2. Paddock Catharine (2012) New clue to how cancer cells spread. MNT Knowledge Center. http://www.medicalnewstoday.com/articles/251306.php
3. Vicent S, Luis-Ravelo D, Antón I, Hernández I, Martínez S, de las Rivas J, Gúrpide A, Lecanda F (2006) Las metástasis óseas del cáncer. Anales del Sistema Sanitario de Navarra. 29(2). http://scielo.isciii.es/scielo.php?script=sci_arttext&pid=S1137-66272006000300002
4. Tashiro H, Brenner MK (2017) Immunotherapy against cancer-related viruses. Cell Research 27:59–73. https://doi.org/10.1038/cr.2016.153 http://www.nature.com/cr/journal/v27/n1/full/cr2016153a.html
5. Morgan RA, Dudley ME et al (2006) Cancer regression in patients after transfer of genetically engineered lymphocytes. Science 314(5796):126-129. https://doi.org/10.1126/science.1129003. http://science.sciencemag.org/content/314/5796/126?variant=full-text&sso=1&sso_redirect_count=1&oauth-code=5cd56f06-ffb4-4ce1-bf7d-6d96585e1e20
6. Liu N, Meng Z, Jia Q, Tan J, Zhang G, Zheng W, Wang R, Li X, Hu T, Upadhyaya A, Zhou P, Wang S (2016) Multiple-factor analysis of the first radioactive iodine therapy in post-operative patients with differentiated thyroid cancer for achieving a disease-free status. Sci Rep 6:34915. https://doi.org/10.1038/srep34915. http://www.nature.com/articles/srep34915
7. Nwatsock JF et al (2012) Radioiodine thyroid ablation in graves' hyperthyroidism: merits and pitfalls. World J Nucl Med 11(1):7–11. https://doi.org/10.4103/1450-1147.98731 http://www.ncbi.nlm.nih.gov/pmc/articles/PMC3425234/?report=classic
8. Liao L, Liu J, Dreaden EC, Morton SW, Shopsowitz KE, Hammond PT, Johnson JA (2014) Convergent synthetic platform for single-nanoparticle combination cancer therapy: Ratiometric loading and controlled release of cisplatin, doxorubicin, and camptothecin. J Am Chem Soc 136(16):5896–5899. https://doi.org/10.1021/ja502011g http://pubs.acs.org/doi/abs/10.1021/ja502011g
9. Babu PJ, Saranya S, Mallepogu V (2015) Nanoformulations as drug delivery vehicles for cancer treatment. Austin J Nanomed Nanotechnol 3(1):1038
10. Misra SK, Ostadhossein F, Daza E, Johnson EV, Pan D (2016) Hyperspectral imaging offers visual and quantitative evidence of drug release from zwitterionic-phospholipid-nanocarbon when concurrently tracked in 3D intracellular space. Adv Funct Mater 26:8031–8041
11. Hong SY, Tobias G (2010) Filled glycosylated carbon nanotubes for in vivo radioemitter localization and imaging. Nat Mater 9:485–490. https://doi.org/10.1038/nmat2766
12. Martinčić M, Pach E, Ballesteros B, Tobias G (2013) Filling of single-walled and multi-walled carbon nanotubes with inorganic payloads. NanoMedicine School. Abstract Collection, University of Trieste. http://www.dscf.units.it/nms2013/Abstract_files/NMS2013%20Abstract%20collection.pdf
13. Umran NM et al (2015) Study of endohedral doped C_{60} fullerene using model potentials. Mater Res Express 2:055603. https://doi.org/10.1088/2053-1591/2/5/055603
14. Valderrama A, Guzmán J (2014) Encapsulation of sodium radio-iodide in fullerene C_{60}. J Molec Model 20:2130. https://doi.org/10.1007/s00894-014-2130-y
15. Valderrama A, Reynoso R, Gómez RW, Marquina V (2016) Self-stability of C_{60} nanocapsules with radio-iodide content and its interaction with calcium atoms. J Mol Model https://doi.org/10.1007/s00894-015-2898-4. http://link.springer.com/article/10.1007%2Fs00894-015-2898-4
16. Walther JH, Jaffe R, Halicioglu T, Koumoutsakos (2001) Carbon nanotubes in water: structural characteristics and energetics. Chem Phys B 105:9980. https://doi.org/10.1021/jp011344u.
17. Popadić A, Praprotnik M, Koumoutsakos P, Walther JH (2015) Continuum simulations of water flow past fullerene molecules. Europ Phys J Spec Top. https://doi.org/10.1140/epjst/e2015-02414-y http://link.springer.com/article/10.1140%2Fepjst%2Fe2015-02414-y
18. Jaffe RL, Walther JH, Kotsalis E, Werder T, Halicioglu PT (2013) Molecular dynamics simulations of fullerenes and carbon nanotubes in water. NASA Ames Research Center. http://www.electrochem.org/dl/ma/201/pdfs/0937.pdf
19. Valderrama A, Reynoso R, Gómez RW et al (2017) Interactions of calcium with the external surfaces of fullerenes and endofullerenes doped with radioactive sodium iodide. J Mol Model 23:15. https://doi.org/10.1007/s00894-016-3187-6
20. Bartelmess J, Giordani S (2014) Carbon nano-onions (multi-layer fullerenes): chemistry and applications. Beilstein J Nanotechnol 5:1980–1998. https://doi.org/10.3762/bjnano.5.207
21. Kostarelos K (2008) The long and short of carbon nanotube toxicity. Nat Biotechnol 26(7):774–776. https://doi.org/10.1038/nbt0708-774
22. Ghorbanzadeh Ahangari M, Fereidoon A, Darvish Ganji M, Sharifi N. Density functional theory based molecular dynamics simulation study on the bulk modulus of multi-shell fullerenes. Physica B: Condensed Matter 423(15):1–5. http://www.sciencedirect.com/science/article/pii/S0921452613002664
23. Parr RG, Yang W (1989) Density-functional theory of atoms and molecules. Oxford University Press, Oxford, pp 76-77. https://es.scribd.com/doc/124889930/Density-functional-theory-of-atoms-and-molecules
24. Hohenberg P, Kohn W (1964) Inhomogeneous electron gas. Phys Rev 136:B864–B871 http://users.wfu.edu/natalie/s15phy752/lecturenote/HohenbergPhysRev.136.B864.pdf
25. Runge E, Gross EKU (1984) Density-functional theory for time-dependent systems. Phys Rev Lett 52(12):997–1000. https://doi.org/10.1103/PhysRevLett.52.997 http://journals.aps.org/prl/abstract/10.1103/PhysRevLett.52.997
26. Marx D, Hutte J (2000) Ab initio molecular dynamics: theory and implementation. Modern methods and algorithms of quantum chemistry. In: Grotendorst J (ed) NIC Series, vol. 1. John von Neumann Institute for Computing, Jülich, pp 301–449 http://www.theochem.ruhr-uni-bochum.de/research/marx/marx.pdf
27. Giannozzi P, Baroni S, Bonini N, Calandra M, Car R, Cavazzoni C et al (2009) Quantum ESPRESSO: a modular and open-source software project for quantum simulations of materials. J Phys Condens Matter 21:395502–395519 http://www.quantum-espresso.org/news/1494/
28. Perdew JP, Burke K, Ernzerhof M (1996) Generalized gradient approximation made simple. Phys Rev Lett 77:3865–3868. http://journals.aps.org/prl/abstract/10.1103/PhysRevLett.77.3865
29. Giannozzi P (2016) Notes on pseudopotential generation. Scuola Normale Superiore di Pisa. http://www.quantum-espresso.org/wp-content/uploads/Doc/pseudo-gen.pdf
30. Troullier N, Martíns JL (1991) Efficient pseudo potentials for plane-wave calculations. Phys Rev B 43:1993–2006 http://journals.aps.org/prb/abstract/10.1103/PhysRevB.43.1993
31. Methfessel M, Paxton A (1989) High-precision sampling for Brillouin-zone integration in metals. Phys Rev B 40:3616. https://doi.org/10.1103/PhysRevB.40.3616 https://journals.aps.org/prb/abstract/10.1103/PhysRevB.40.3616
32. González-Hernández R, López-Pérez W, Moreno-Armenta MG, Rodríguez JA (2010) Vanadium adsorption and incorporation at the GaN(0001) surface: a first-principles study. Phys Rev B 81:195407. https://journals.aps.org/prb/abstract/10.1103/PhysRevB.81.195407

33. Timon V, Brand S, Clark SJ, Abram RA. Theoretical adlayer surface morphology of wurtzite 2 × 2 reconstructions of the GaN(0001) surface. J Phys: Condens Matter 17:17–26. http://iopscience.iop.org/article/10.1088/0953-8984/17/1/002
34. Parrinello M, Rahman A (1981) Polymorphic transitions in single crystals a new molecular dynamics method. J Appl Phys 52:7182 http://adsabs.harvard.edu/abs/1981JAP....52.7182P
35. Hare J et al (2013) Some properties of carbon and C60. Brighton, East Sussex BN1 9QJ. Accessed January 2013. http://www.creative-science.org.uk/propc60.html
36. Yoon M et al (2008) Calcium as the superior coating metal in functionalization of carbon fullerenes for high-capacity hydrogen storage. Phys Rev Lett 100:206806 http://journals.aps.org/prl/abstract/10.1103/PhysRevLett.100.206806
37. Scientific Computing & Modelling (2014) ADF program system. NV Vrije Universiteit, theoretical chemistry de Boelelaan, Amsterdam, The Netherlands. http://www.scm.com/Doc/Doc2014/ADF/ADFUsersGuide/page319.html